Microstructural and Hardness Study of Pulsed Nd:YAG Laser Surface Alloyed Aluminum with Iron

MOHAMMAD ANSARI, REZA SOLTANI , MAHMOUD HEYDARZADEH SOHI, and ZIA VALEFI

In the present study, the feasibility of the formation of surface layers containing hard iron aluminides on AA6061-T6 aluminum *via* pre-plasma spraying with iron and subsequently double surface melting by pulsed Nd:YAG laser is studied. The effects of single and double laser surface melting on microstructure, phase formation, and hardness of the treated layers are examined. Single-step laser treatment resulted in the presence of undissolved iron particles surrounded by lump-like Al_5Fe_2 and needle-like Al_3Fe intermetallic compounds. Double laser surface melting dissolved the retained undissolved irons and resulted in the formation of Al-Al_3Fe eutectic structure. Microhardness profiles along cross section and top surface of the treated layers indicated that laser surface alloying with iron enhanced the hardness of the aluminum to more than twice of that of the base material.

DOI: 10.1007/s11661-015-3320-7

I. INTRODUCTION

LIQUID-PHASE surface treatment by means of laser, electron beam, and other heat sources has widely been examined and applied on aluminum alloys.[1–4] It has been reported that surface alloying of aluminum with transition metals (TM) like nickel, chromium, tungsten, molybdenum, and iron resulted in the formation of Al_xTM_y intermetallics, along with structural modification, and thereby, improved surface properties like hardness, corrosion, and wear resistance. Heydarzadeh Sohi[5] investigated electron beam surface alloying of LM13 aluminum with nickel. The results showed a significant increase in hardness and wear life of LM13 aluminum alloy owing to the formation of hard Al_3Ni intermetallic phase. Ansari *et al.*[6] investigated pulsed Nd:YAG laser surface alloying of AA6061 aluminum with chromium and showed this treatment resulted in the formation of Al_7Cr and Al_4Cr intermetallic phases on the surface of AA6061 aluminum, and as a result, an improvement in surface hardness was obtained. Rajamure *et al.*[7] studied the corrosion resistance of laser surface alloyed AA1100 aluminum with tungsten and reported a substantial improvement in corrosion resistance of AA1100 aluminum due to the formation of Al_4W intermetallic phase. In another study, Rajamure *et al.*[8] investigated wear behavior of laser surface alloyed AA1100 aluminum with molybdenum and reported enhancement in wear resistance due to the formation of Al_8Mo_3 and Al_5Mo intermetallic phases.

Liquid-phase surface alloying of aluminum with iron using laser beam has been reported in a couple of articles. Gjønnes and Olsen[9] investigated the effects of two different CO_2 laser beam settings on hardness and microstructure of surface alloyed 5000-aluminum alloy with iron and reported an improvement in hardness owing to the formation of Al_3Fe intermetallic phase. In another study, Tomida and Nakata[10] reported enhanced surface hardness and wear resistance of Fe-Al composite layer on AA5052 aluminum plate through application of CO_2 laser surface alloying. In these researches, laser surface alloying of aluminum was carried out using continuous wave CO_2 lasers. Metallic materials reflect a major portion of the laser energy (reflectivity $\gg 1$ for far infrared at $\lambda = 10$ μm). CO_2 laser with its long wavelength (10.6 μm) suffers from poor absorption during materials' interaction, especially for aluminum, which has high reflectivity. It is, therefore, advised to use laser beams with short wavelength for liquid-phase surface treatment of metals, particularly for the case of aluminum base materials. The radiation of $\lambda = 1$ μm is less reflected. Thus, Nd:YAG laser with short wavelength of 1.06 μm benefits from higher energy absorption, which increases processing efficiency compared to CO_2 laser.[11]

Figure 1 shows parts of the binary Al-Fe-phase diagram (0 to 55 wt pct Fe), which was computed by Thermo-Calc™ software. Iron has a low solubility in solid-state aluminum (~0.04 pct) and the iron content in aluminum alloys generally appears as intermetallic phases.

Possibility of the formation of Al-Fe intermetallics in the reaction between liquid aluminum and solid iron has been studied in a number of researches. However, the

MOHAMMAD ANSARI, Research Assistant, REZA SOLTANI, Assistant Professor, and MAHMOUD HEYDARZADEH SOHI, Professor, are with the School of Metallurgy and Materials Engineering, College of Engineering, University of Tehran, P.O. Box 11155-4563, Tehran, Iran. Contact e-mail: rsoltani@ut.ac.ir ZIA VALEFI, Assistant Professor, is with Malek-Ashtar University of Technology, Tehran, Iran.

Manuscript submitted June 22, 2015.
Article published online January 12, 2016

formation priority among various aluminum-rich intermetallics could thermodynamically and kinetically be affected. It has been reported in the literature that the main intermetallics formed in reaction between aluminum and iron are Al_5Fe_2 and Al_3Fe phases. Shahverdi *et al.*[12] studied interfacial reaction between solid iron and liquid aluminum and identified the phases to be Al_5Fe_2 and Al_3Fe. Bouché *et al.*[13] studied the interaction between solid iron and liquid aluminum by immersion tests and approved the formation of Al_5Fe_2 and Al_3Fe phases, theoretically and experimentally. Lee *et al.*[14] revealed the sequences of the formation of Al_5Fe_2 and Al_3Fe phases on the reaction between solid iron and liquid aluminum by the plasma synthesis method.

Having considered the different natures of the continuous wave CO_2 and pulsed Nd:YAG lasers, and hence their effects on the characteristics of the treated layers, surface alloying of AA6061-T6 aluminum *via* pre-plasma spraying with iron and subsequently double-pulsed Nd:YAG laser melting are studied. The effects of laser surface alloying (single-step melting) and re-melting (double step melting) on microstructure, phase formation, and hardness of the surface-treated specimens are investigated.

II. EXPERIMENTAL PROCEDURE

AA6061-T6 aluminum-based specimens with dimensions 50 mm × 30 mm × 5 mm were used as the sublayer. High purity iron powder with particle size distribution of 30 to 40 μm was initially deposited on the surface of the grit-blasted AA6061-T6 aluminum specimens by Air Plasma Spray process (A3000S, Plasma Technik, AG). The Plasma Spray parameters are given in Table I. Figure 2 shows the morphology of the iron powders and cross-sectional SEM view of the pre-sprayed specimen. The thickness of the deposited layer was about 30 to 50 μm.

The pre-sprayed specimens were irradiated with a 400 W-pulsed Nd:YAG laser (model IQL-10) in a near TEM_{00} mode at optimum process parameters such as average power of 240 W and scanning speed of 8 mm/s (energy density of 6.1 J/mm^2) with about 30 pct longitudinal spot overlap under pure argon gas shield. The as-alloyed layer were re-melted (double-step laser melting) in the same direction as single-step melting process at an average power of 240 W and scanning speed of 2 mm/s (energy density of 24.4 J/mm^2) with about 80 pct longitudinal spot overlap under pure argon gas

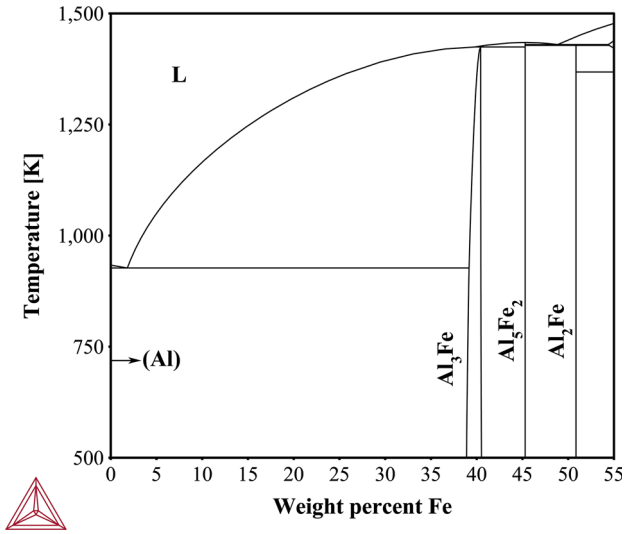

Fig. 1—Partial Al-Fe phase diagram.

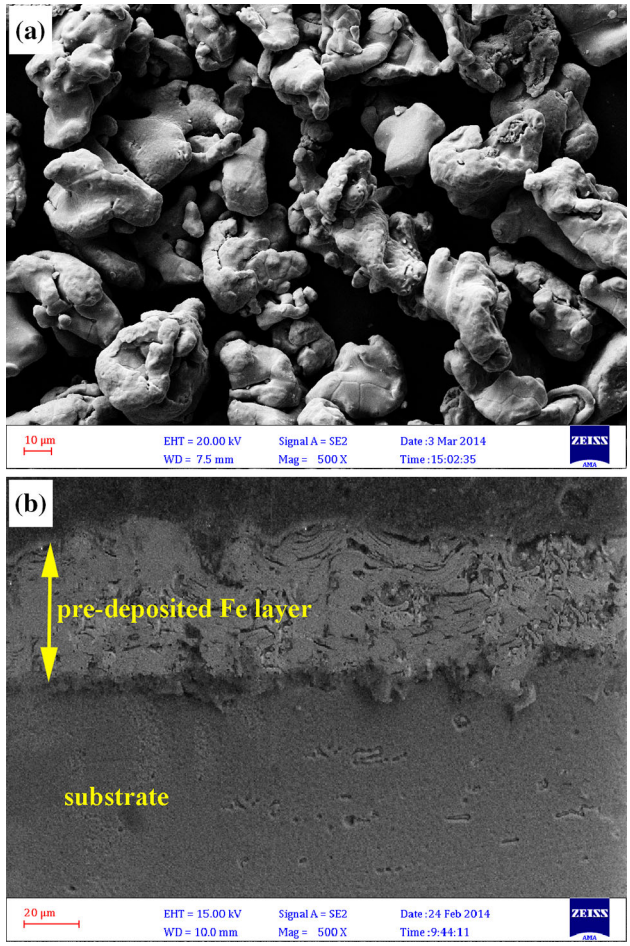

Fig. 2—SEM micrograph of (*a*) iron powders and (*b*) cross-sectional view of pre-sprayed specimen.

Table I. Air Plasma Spray Parameters Used for Deposition of Iron

Gun	Stand-off Distance	Carrier Gas Flow Rate (Ar)	Powder Feed Rate	Voltage	Current	Primary Plasma Gas (Ar)	Secondary Plasma Gas (H_2)
Sulzer metco F4	12 cm	3 L/min	30 g/min	63 V	600 A	45 L/min	12 L/min

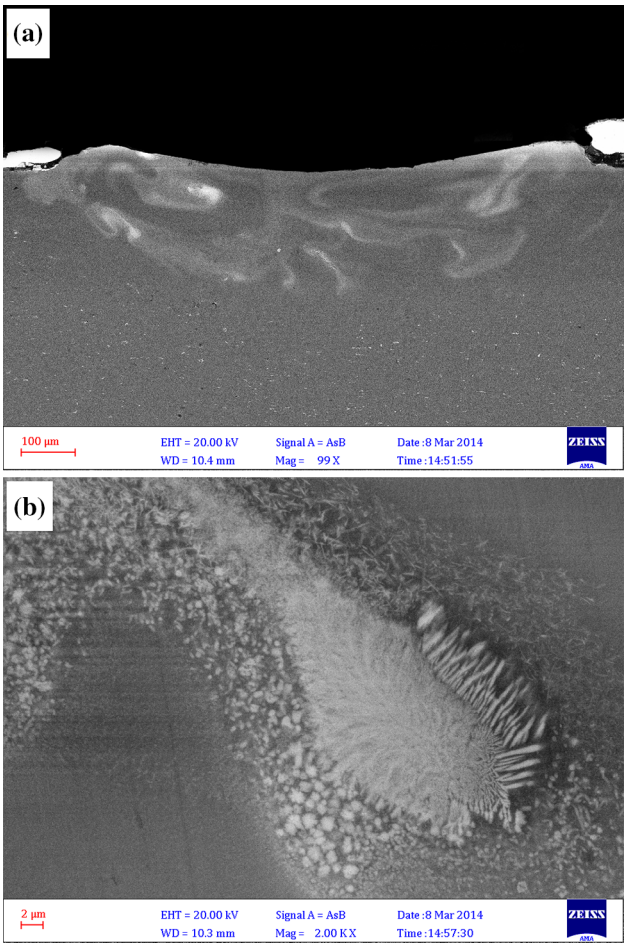

Fig. 3—(*a*) Low and (*b*) high magnification cross-sectional backscattered SEM micrographs of as-alloyed layer achieved at average power of 240 W and scanning speed of 8 mm/s.

shield. Laser re-melting of the as-alloyed layers can eliminate and minimize non-uniformity in composition and microstructure, especially when alloying elements with high melting points (like iron) are used.[15,16] Other laser parameters such as defocusing distance, defocused beam diameter, pulse duration, and frequency were fixed at 4 mm, 0.75 mm, 8 ms, and 15 Hz, respectively.

The laser surface alloyed specimens were studied using standard metallographic techniques and etched with Keller's reagent. The microstructural evaluation and chemical composition of the alloyed layers were examined by FE-SEM (ΣIGMA VP, ZEISS) electron imaging equipped with an energy dispersive X-ray spectrometry (EDS) analyzer. Phase identification of surface layers was carried out by X-ray diffraction (X' Pert Pro, Phillips) using Cu Kα radiation at 40 kV, 30 mA, and scanned within $2\theta = 20$ to 50 deg. Microhardness Vickers machine (W-432SVD, Buehler) was used at a load of 100 gf and a loading time of 15 seconds to measure hardness along the polished cross section and top surface of the treated layer. The microhardness measurements were average values of three to five indentions at the same depth from the surface (along the cross section) and the same distance from the laser track center (along the top surface).

III. RESULTS AND DISCUSSION

A. *Microstructural and Phase Analysis*

Figure 3(a) shows backscattered cross-sectional SEM micrograph of the as-alloyed layer produced by laser surface alloying at average power of 240 W and scanning speed of 8 mm/s, which reveals heterogeneous layer with iron-rich areas. Depth and width of the surface layer were about 230 and 1170 μm, respectively. Higher magnification backscattered SEM micrograph of this layer is shown in Figure 3(b). This figure also clearly shows large lump-like iron-rich areas in the treated layer, which are surrounded by ultra-fine intermetallic compounds.

Figure 4 shows low and high magnification backscattered top view SEM micrographs of as-alloyed layer. The top view of as-alloyed layer is also heterogeneous and contains pores and undissolved iron particles (Figure 4(a)). Figure 4(b) shows undissolved iron particles, which are surrounded by partially reacted lump-like and needle-like intermetallic compounds. Theoretically, according to the Al-Fe binary diagram (see Figure 1), the Al_5Fe_2 intermetallic exists in the range of 43 to 47 wt pct Fe, the Al_3Fe intermetallic exists in the range of 38.7 to 41.5 wt pct Fe, and eutectic structure of Al-Al_3Fe can totally or partially exist in the range of 0 to 38.7 wt pct Fe. According to detailed EDS spot analysis (Figure 4(b)), region 1 with 99 wt pct iron is undissolved pure iron, region 2 with 46 wt pct Fe is Al_5Fe_2 intermetallic with lump-like morphology, and region 3 (Figure 4(c)) with needle-like morphology and 28 wt pct Fe has eutectic structure of Al-Al_3Fe. Furthermore, micro-cracks are noticed at interface of undissolved iron and Al_5Fe_2 phase.

The presence of undissolved iron and partially reacted particles is due to the following two reasons: First, liquid homogenization of melt before solidification requires mass transport by Marangoni convection as explained by Almeida and Vilar.[17] The low temperature coefficient of surface tension of AA6061 aluminum that reported by Bainbridge and Taylor[18] as well as the short lifetime of the melt pool and moderate Marangoni convection lead to insufficient homogenization of melt. In fact, the moderate convection is not enough for the formation of a homogenized liquid before solidification and thus undissolved iron and partially reacted particles remained. Second, undissolved iron particles are surrounded by layers of high melting point intermetallic compounds (Al_5Fe_2 and Al_3Fe) and slow down dissolution kinetics, since it is then controlled by diffusion in solid-state throughout the layer instead of fairly faster mass transport in liquid.

Furthermore, Al_5Fe_2 intermetallic at temperatures below 773 K (500 °C) is totally brittle, as discussed by Hirose *et al.*,[19] and has different atomic volumes and expansion coefficients from undissolved iron particles. Therefore, their presence at the interface between undissolved iron particles and aluminum matrix leads to the nucleation of cracks at the interface of undissolved iron particles/Al_5Fe_2 intermetallic, which spread through the Al_5Fe_2 intermetallic compound (Figure 4(b)). These

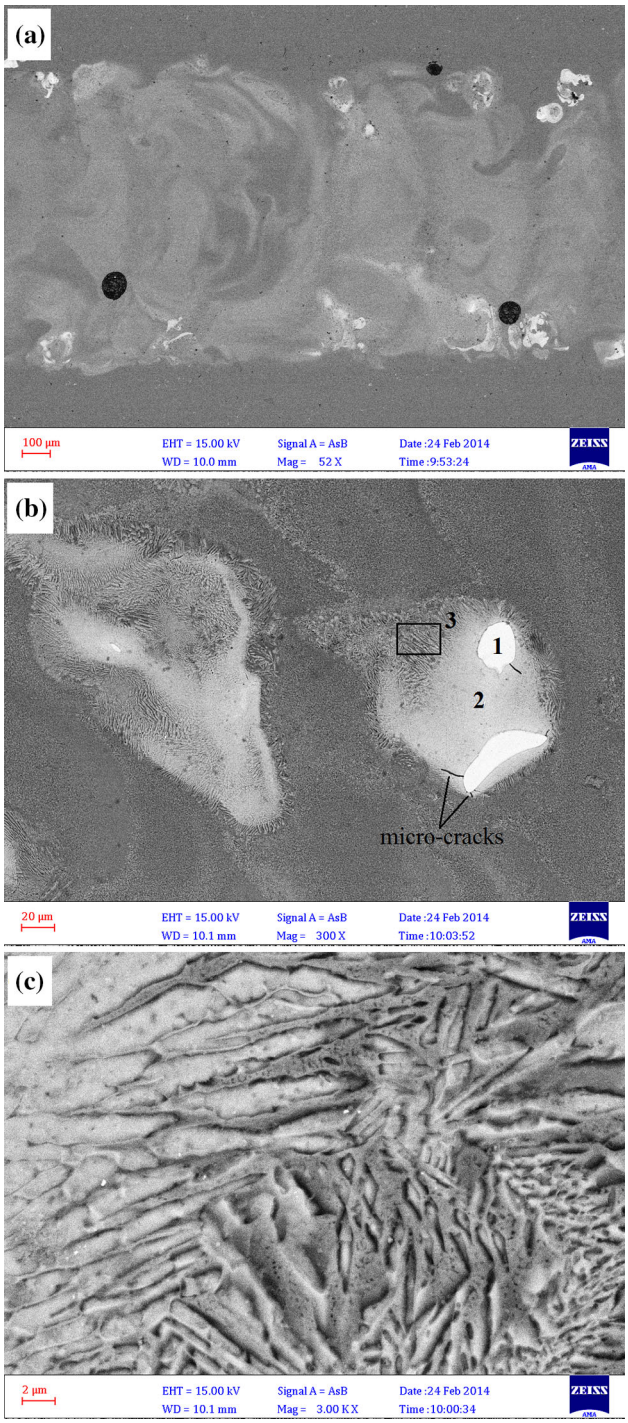

Fig. 4—(*a*) Low and (*b*) high magnification backscattered SEM micrographs of top view of as-alloyed layer at an average power of 240 W and scanning speed of 8 mm/s, and (*c*) high magnification backscattered SEM micrographs of region 3 in Fig. 4b.

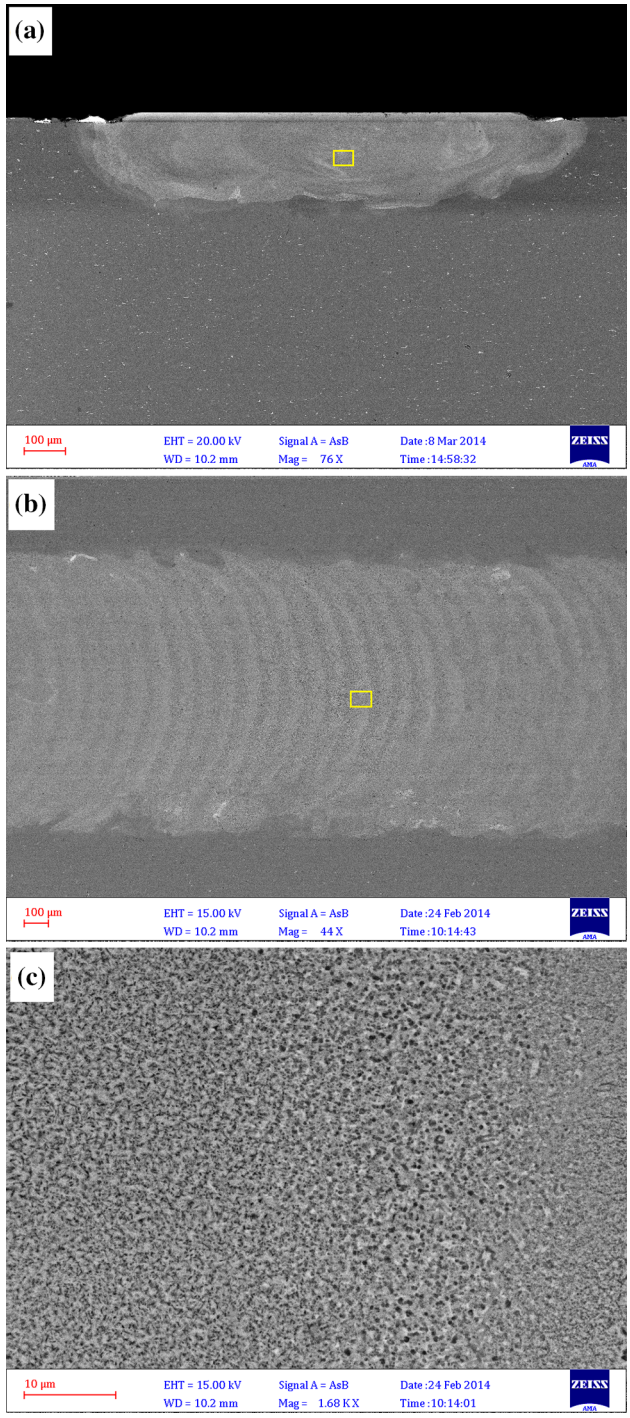

Fig. 5—Backscattered SEM micrographs of (*a*) cross section, (*b*) top view of re-melted layer achieved at average power of 240 W and scanning speed of 2 mm/s, and (*c*) high magnification backscattered SEM micrographs of the selected region shown in Fig. 5b.

undissolved iron and partially reacted intermetallic particles are particularly harmful to the performance of alloyed layers. Use of the laser re-melting can help to minimize these defects.

Figure 5 shows backscattered cross-sectional and top view SEM micrographs of the re-melted layer achieved at average power of 240 W and scanning speed of 2 mm/s. Since, undissolved iron and partially reacted intermetallic particles have high melting temperatures, lower laser scanning speed (2 mm/s) was chosen for re-melting process to increase input energy and improve homogeneity. After laser re-melting, the pores, micro-cracks, and iron-rich areas were eliminated and an almost flat surface layer with more or less homogeneous microstructure was

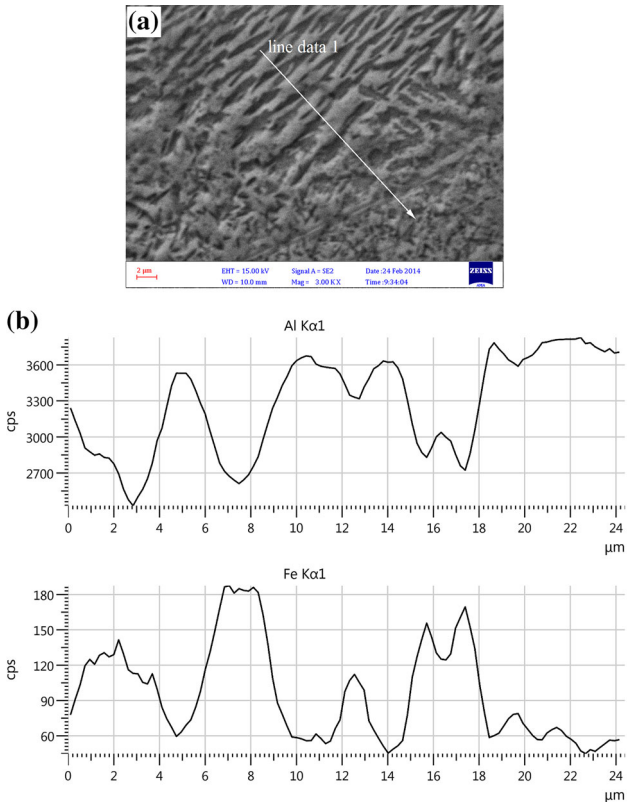

Fig. 6—(*a*) High magnification cross-sectional SEM micrograph of the selected region shown in Fig. 5a, and (*b*) EDS analysis of the line selected in Fig. 6a.

obtained (Figures 5(a) and (b)). However, slight banding effect in the re-melted structure can be observed that is typical of the laser-melted layer and it is almost inevitable. Figure 5(c) also shows high magnification top view SEM micrograph of the re-melted layer consisted of fine needle-like structure, which is believed to be Al_3Fe intermetallic. Laser re-melting process did not change the geometry of the alloyed layer, significantly. Depth and width of the surface re-melted layer were about 240 and 1240 μm, respectively.

Figure 6(a) shows high magnification cross-sectional SEM micrographs of the re-melted layer that consisted of coarse and fine needle-like structures. A couple of other works have also reported similar observations.[9,10] According to EDS line analysis (Figure 6(b)), iron- and aluminum-rich layers nucleate and grow next to each other, which is characteristic of eutectic structures. Therefore, the microstructure of re-melted layer consisted of acicular eutectic structure of Al-Al_3Fe.

It is obvious that during laser re-melting, intense Marangoni convection led to enhance liquid homogenization of melt and dissolve retained iron and large intermetallic particles. Since, the input energy, Marangoni convection, and laser-material interaction time are increased with decreasing laser scanning speed, the liquid has a longer solidification time duration for more mass transport and liquid homogenization by a more intense Marangoni stirring convection during the re-melting process. In addition, more or less complete

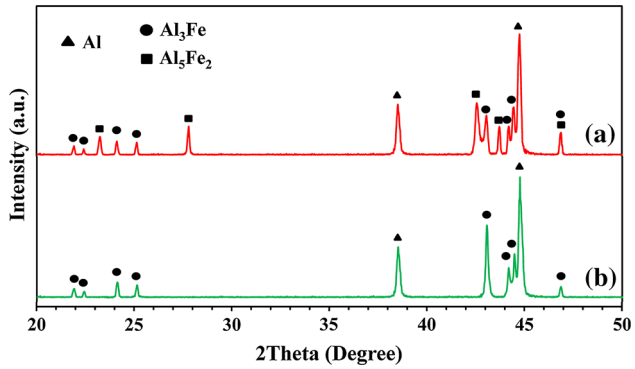

Fig. 7—X-ray diffraction patterns of (*a*) as-alloyed and (*b*) re-melted layers.

and uniform dissolution of the retained iron and partially reacted intermetallic particles can occur in the re-melted layer.

Figure 7 shows the XRD patterns of the as-alloyed and re-melted layers. In spite of the proximity of the peaks of the Al-Fe intermetallics, all phases were clearly identified. Pattern of the as-alloyed layer confirmed that this layer consisted of Al, Al_3Fe, and Al_5Fe_2 phases. The microstructure of this layer also indicated the formation of these phases (Figures 3(b), 4(b), and (c)). Nevertheless, pattern of the re-melted layer indicated that this layer only consisted of Al and Al_3Fe phases, which was confirmed by the microstructure of this layer in Figure 6. It is noticeable that there were not any Al_5Fe_2 and iron phases in XRD pattern of re-melted layer. Since, the iron peaks overlap the aluminum peaks, iron peaks cannot be detected from the X-ray diffraction patterns.

The thermodynamic behavior of Al-Fe binary system is an important reason for the formation of Al_3Fe and Al_5Fe_2 intermetallic compounds. Based on Gibbs free energy, among all possible intermetallic compounds, the intermetallic compound with lowest Gibbs free energy has highest tendency to occur. Gibbs free energy as a function of composition for Al-Fe intermetallic phases are shown in Figure 8, which were computed at 298 K (25 °C) according to thermodynamic study of other works.[20–22] As shown in Figure 8, the Gibbs free energy of formation of the Al_3Fe and Al_5Fe_2 intermetallic compounds is far lower than other intermetallics, which indicates that formation of Al_3Fe and Al_5Fe_2 compounds are preferred.

According to recent comprehensive study by Lee *et al.*[14] on reaction between solid iron and liquid aluminum, the sequences of the formation of intermetallics are as follows: (i) Fe dissolve into the aluminum melt until its concentration reaches to the maximum solubility. The dissolved iron leads to the formation of needle-like Al_3Fe during solidification. (ii) Al_3Fe initially forms at the interface of liquid aluminum/solid iron. (iii) Al_3Fe decomposes to form Al_5Fe_2 at the interface of Al_3Fe/Fe. Al_5Fe_2 then grows toward the iron particle due to its higher growth velocity as compared with Al_3Fe. (iv) Al_3Fe separates from Al_3Fe/Al_5Fe_2 layer due to heat extraction caused by the

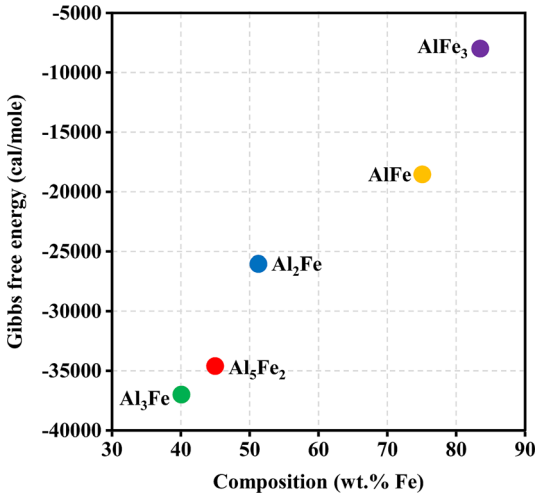

Fig. 8—Gibbs free energy as a function of composition for various Al-Fe intermetallic phases at 298 K (25 °C).

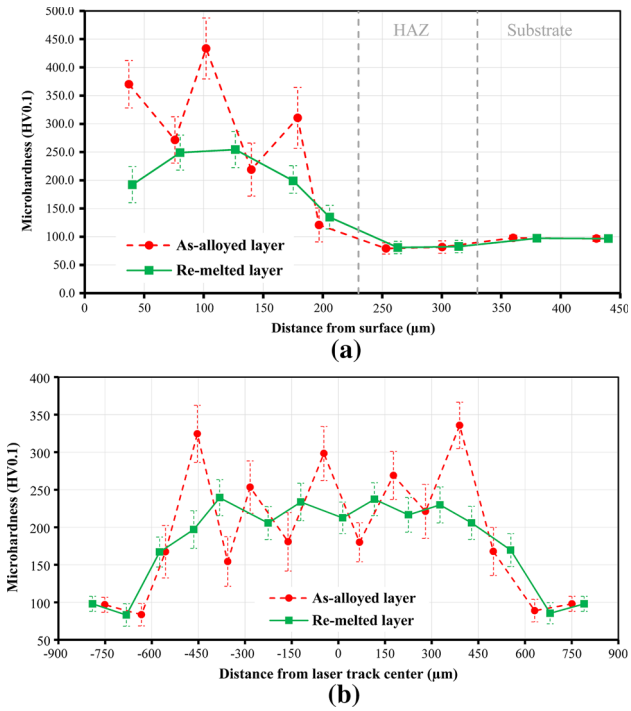

Fig. 9—Hardness profiles along (*a*) cross section and (*b*) top surface of as-alloyed and re-melted layers.

reaction and induced stirring movement. (v) New Al_3Fe forms in the fresh Al/Al_5Fe_2 layer. (vi) Steps (iv) and (v) repeat and result in complete reaction of iron and formation of Al_3Fe in the matrix.

On the whole, it appears that the present work is somehow in agreement with the recent study by Lee *et al.*[14] During the first step of melting, short solidification time and moderate convection caused the undissolved iron particles to be seen that were surrounded by partially reacted lump-like Al_5Fe_2 and needle-like Al_3Fe intermetallic compounds (sequences (i)-(iii)). Re-melting

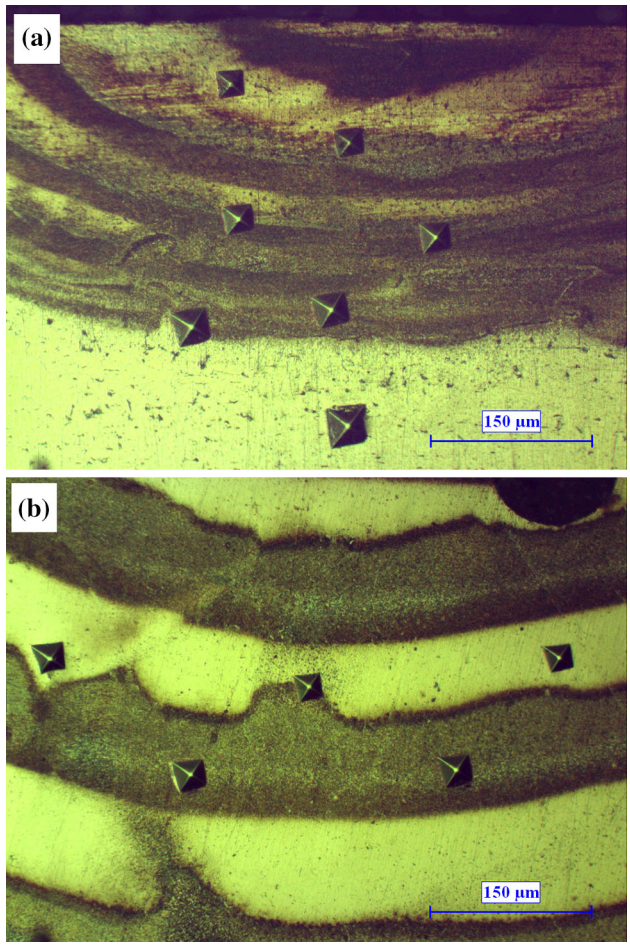

Fig. 10—Optical micrographs showing the microhardness indentations along the cross section (*a*) and top surface (*b*) of the re-melted layer.

associated with intense Marangoni stirring convection and more liquid homogenization due to long interaction time resulted in complete reaction of Al and Fe, and hence, the formation of Al_3Fe in aluminum matrix (sequences (iv)-(vi)) took place.

B. *Microhardness*

Figures 9(a) and (b), respectively, show cross-sectional hardness profiles from surface toward substrate and the hardness profiles along the polished top surface for the as-alloyed and re-melted layers. The high hardness fluctuation with high standard deviation for the case of as-alloyed layer in Figure 9 is in harmony with the heterogeneity in microstructure of single-step laser-melted layer, which is clearly seen in Figures 3(a), (b), 4(a), and (b). The smooth hardness profile for the re-melted layer is also justified with its more or less uniform microstructure shown in Figures 5(a) through (c). These hardness profiles also indicate that the hardness in laser-alloyed zones were over 4 and 2 times higher than that of the aluminum substrate (95 HV) for the as-alloyed and re-melted layers, respectively.

Furthermore, the hardness of as-alloyed layer was about twice as high as that for the re-melted layer and exhibited large fluctuation. This is mainly attributed to the presence of the harder undissolved iron and large Al_5Fe_2 intermetallic particles in the as-alloyed layer (see Figures 3(b) and 4(b)). As was mentioned before, laser re-melting resulted in dissolution of these particles and led to a more and less uniform hardness distribution. Re-melting reduced the hardness due to the formation of eutectic Al-Al_3Fe structure with lower hardness than undissolved iron and large Al_5Fe_2 intermetallic particles. It should be noticed that bulk Al_5Fe_2 phase is harder than bulk Al_3Fe phase.[23] The optical micrographs given in Figures 10(a) and (b) show the microhardness indentations along the cross section and top surface of the laser re-melted layer, respectively. The fairly equal size of the microhardness indentations could explicitly show the uniform hardness distribution in the laser re-melted layer.

The hardness in the heat-affected zone (HAZ) decreased to about 80 HV. It has been reported that during surface melting of AA6061-T6 aluminum, strengthening Mg_2Si precipitates formed by T6 solution-aging heat treatment on 6061 aluminum dissolve in the aluminum matrix and decrease the hardness in the heat-affected zone.[24,25]

IV. CONCLUSIONS

Laser surface alloying and re-melting of AA6061-T6 aluminum with preplaced iron powder was successfully performed using a pulsed Nd:YAG laser and the following results were achieved:

1. The as-alloyed layer demonstrated heterogeneous microstructure consisting of undissolved iron particles, which were surrounded by partially reacted lump-like Al_5Fe_2 intermetallics with micro-cracks at their interface and needle-like Al_3Fe intermetallic in the α-Al matrix.
2. The laser re-melting considerably eliminated the defects and demonstrated homogeneous microstructure consisting the acicular eutectic structure of Al-Al_3Fe.
3. The hardness of as-alloyed layer due to the presence of undissolved iron and partially reacted particles exhibited fourfold value compared with that of the substrate, with large fluctuation.
4. Laser re-melting resulted in the formation of a fairly smooth and defect-free alloyed layer with more or less uniform hardness distribution (twice of that of the substrate) owing to the presence of Al-Al_3Fe eutectic structure.

REFERENCES

1. M. Heydarzadeh Sohi, M. Ansari, M. Ghazizadeh, and H. Zebardast: *Surf. Eng.*, 2015, vol. 31, pp. 598–604, DOI:10.1179/1743294414Y.0000000372.
2. H. Wang, W. Jiang, J. Ouyang, and R. Kovacevic: *J. Mater. Process. Technol.*, 2004, vol. 148, pp. 93–102, DOI:10.1016/j.jmatprotec.2004.01.058.
3. S. Katakam, S.S. Joshi, S. Mridha, S. Mukherjee, and N.B. Dahotre: *J. Appl. Phys.*, 2014, vol. 116, p. 104906, DOI:10.1063/1.4895137.
4. M.M. Quazi, M.A. Fazal, A.S.M.A. Haseeb, F. Yusof, H.H. Masjuki, and A. Arslan: *Crit. Rev. Solid State Mater. Sci.*, 2015, DOI:10.1080/10408436.2015.1076716.
5. M. Heydarzadeh Sohi: *J. Mater. Process. Technol.*, 2001, vol. 118, pp. 187–92, DOI:10.1016/S0924-0136(01)00912-8.
6. M. Ansari, M. Heydarzadeh Sohi, R. Soltani, and M.J. Torkamany: *Int. J. Adv. Manuf. Technol.*, 2015, DOI:10.1007/s00170-015-7516-1.
7. R.S. Rajamure, H.D. Vora, S.G. Srinivasan, and N.B. Dahotre: *Appl. Surf. Sci.*, 2015, vol. 328, pp. 205–14, DOI:10.1016/j.apsusc.2014.12.037.
8. R.S. Rajamure, H.D. Vora, N. Gupta, S. Karewar, S.G. Srinivasan, and N.B. Dahotre: *Surf. Coatings Technol.*, 2014, vol. 258, pp. 337–42, DOI:10.1016/j.surfcoat.2014.08.074.
9. L. Gjønnes and A. Olsen: *J. Mater. Sci.*, 1994, vol. 29, pp. 728–35, DOI:10.1007/BF00445986.
10. S. Tomida and K. Nakata: *Surf. Coatings Technol.*, 2003, vols. 174–175, pp. 559–63, DOI:10.1016/S0257-8972(03)00698-4.
11. S. Zhang and D. Zhao, eds.: *Aerospace Materials Handbook*, CRC Press, Boca Raton, 2012, p. 112.
12. H.R. Shahverdi, M.R. Ghomashchi, S. Shabestari, and J. Hejazi: *J. Mater. Process. Technol.*, 2002, vol. 124, pp. 345–52, DOI:10.1016/S0924-0136(02)00225-X.
13. K. Bouché, F. Barbier, and A. Coulet: *Mater. Sci. Eng. A*, 1998, vol. 249, pp. 167–75, DOI:10.1016/S0921-5093(98)00573-5.
14. J. Lee, S. Kang, T. Sato, H. Tezuka, and A. Kamio: *Mater. Sci. Eng. A*, 2003, vol. 362, pp. 257–63, DOI:10.1016/S0921-5093(03)00639-7.
15. W. Gao, S. Zhao, Y. Wang, F. Liu, C. Zhou, and X. Lin: *Mater. Des.*, 2014, vol. 64, pp. 490–96, DOI:10.1016/j.matdes.2014.08.004.
16. S.A. Vaziri, H.R. Shahverdi, S.G. Shabestari, K. Hazeli, and M.J. Torkamany: *Mater. Des.*, 2010, vol. 31, pp. 3875–79, DOI:10.1016/j.matdes.2010.02.040.
17. A. Almeida and R. Vilar: *Lasers Eng.*, 2008, vol. 18, pp. 49–60.
18. I.F. Bainbridge and J.A. Taylor: *Metall. Mater. Trans. A*, 2013, vol. 44A, pp. 3901–09, DOI:10.1007/s11661-013-1696-9.
19. S. Hirose, T. Itoh, M. Makita, S. Fujii, S. Arai, K. Sasaki, and H. Saka: *Intermetallics*, 2003, vol. 11, pp. 633–42, DOI:10.1016/S0966-9795(03)00050-5.
20. E.G. Ivanov: *Met. Sci. Heat Treat.*, 1979, vol. 21, pp. 449–52, DOI:10.1007/BF00780482.
21. R.W. Richards, R.D. Jones, P.D. Clements, and H. Clarke: *Int. Mater. Rev.*, 1994, vol. 39, pp. 191–212, DOI:10.1179/imr.1994.39.5.191.
22. B. Sundman, I. Ohnuma, N. Dupin, U.R. Kattner, and S.G. Fries: *Acta Mater.*, 2009, vol. 57, pp. 2896–2908, DOI:10.1016/j.actamat.2009.02.046.
23. M. Yasuyama, K. Ogawa, and T. Taka: *Weld. Int.*, 1996, vol. 10, pp. 963–70, DOI:10.1080/09507119609549121.
24. A. Hirose, N. Kurosawa, K.F. Kobayashi, H. Todaka, and H. Yamaoka: *Metall. Mater. Trans. A*, 1999, vol. 30A, pp. 2115–20, DOI:10.1007/s11661-999-0022-z.
25. M.J. Cieslak and P.W. Fuerschbach: *Metall. Trans. B*, 1988, vol. 19B, pp. 319–29, DOI:10.1007/BF02654217.